DMD Fast Forward. Published on February 2, 2006 as doi:10.1124/dmd.106.009274

N-Glucuronidation of the PDGF Receptor Tyrosine Kinase Inhibitor 6,7-(Dimethoxy-2,4-dihydroindeno[1,2-c]pyrazol-3-yl)-(3-fluoro-phenyl)-amine by Human UDP-Glucuronosyltransferases

Z. Yan, G.W. Caldwell, D. Gauthier, G. C. Leo, J. Mei, C. Y. Ho, W. J. Jones, J. A. Masucci, R. W. Tuman, R. A. Galemmo, Jr, and D. L. Johnson

Drug Discovery Research

Johnson & Johnson Pharmaceutical Research & Development, LLC

Spring House, PA 19477

Running title:

N-Glucuronidation of 6,7-(Dimethoxy-2,4-dihydroindeno[1,2-c] pyrazol-3-yl)-(3-fluoro-phenyl)-amine

Corresponding Author:

Zhengyin Yan
Drug Discovery
R2013
Johnson & Johnson Pharmaceutical Research & Development, LLC
Welsh & McKean Roads
Spring House, PA 19477-0776

Tel. (215)-628-5036
Fax: (215)-540-4878
E-mail: zyan@prdus.jnj.com

Number of:
- Text Page (with references): 27
- References: 37
- Tables: 6
- Figures: 6

Word count:
- Abstract: 253
- Introduction: 549
- Discussion: 1125

Abbreviations:

UGT: uridine diphosphate glucuronosyltranferase; HLM, human liver microsomes; MLM, monkey liver microsomes; RLM, rat liver microsomes; NMR, nuclear magnetic resonance; LC, liquid chromatography; JNJ-10198409, 6,7-(dimethoxy-2,4-dihydroindeno[1,2-c]pyrazol-3-yl)-(3-fluoro-phenyl)-amine.

DMD Fast Forward. Published on February 2, 2006 as DOI: 10.1124/dmd.106.009274
This article has not been copyedited and formatted. The final version may differ from this version.

Abstract

The potential cancer therapeutic agent, 6,7-(dimethoxy-2,4-dihydroindeno[1,2-c]pyrazol-3-yl)-(3-fluoro-phenyl)-amine (JNJ-10198409), formed three *N*-glucuronides that were positively identified by LC-MS/MS and NMR as *N*-amine-glucuronide (Glu-A), 1-*N*-pyrazole-glucuronide (Glu-B), and 2-*N*-pyrazole-glucuronide (Glu-C). All three *N*-glucuronides were detected in rat liver microsomes, whereas only Glu-A and B were found in monkey and human liver microsomes. In contrast to common glucuronides, Glu-B was completely resistant to β-glucuronidase. Kinetic analyses revealed that glucuronidation of JNJ-10198409 in human liver microsomes exhibited atypical kinetics that may be described by a two-site binding model. For the high affinity binding, K_m values were 1.2 and 5.0 μM, and V_{max} values were 2002 and 2403 nmole min^{-1} mg^{-1} for Glu-A and Glu-B, respectively. Kinetic constants of low affinity binding were not determined due to low solubility of the drug. Among the human UDP-glucuronosyltransferases (UGTs) tested, UGT1A9, 1A8, 1A7 and 1A4 were the most active isozymes to produce Glu-A; for the formation of Glu-B, UGT1A9 was the most active enzyme followed by UGT1A3, 1A7 and 1A4. Glucuronidation of JNJ-10198409 by those UGT1A enzymes followed classic Michaelis-Menten kinetics. In contrast, no glucuronides were formed by all UGT2B isozymes tested, including UGT2B4, 2B7, 2B15 and 2B17. Collectively, these results suggested that glucuronidation of JNJ-10198409 in human liver microsomes is catalyzed by multiple UGT1A enzymes. Since UGT1A enzymes are widely expressed in various tissues, it is anticipated that both hepatic and extra-hepatic glucuronidation will likely contribute to the elimination of the

drug in humans. Additionally, conjugation at the nitrogens of the pyrazole ring represents a new structural moiety for UGT1A-mediated reactions.

Introduction

UDP-glucuronosyltransferases (UGTs) are an important class of biotransformation enzymes that catalyze the glucuronidation of a variety of compounds by transferring a glucuronic acid moiety from the cofactor uridine 5'-diphosphoglucuronic acid (UDPGA) to substrates. Resulting glucuronides are more water-soluble and thus readily excreted via urine or bile. In addition to metabolizing endogenous substrates such as bilirubin and thyroid hormones, UGTs also play an important role in the metabolism of xenobiotics including drugs (King, et al. 2000). UGT enzymes are normally divided into two gene families, UGT1A and UGT2B, based on their sequence homologies (Mackenzie, et al. 1997). UGT1A enzymes have been shown to catalyze glucuronidation of a vast number of substrates at a diverse array of functional groups to form a variety of glucuronides. UGT1A-mediated *N*-glucuronidation represents an important metabolic pathway, as evidenced by the fact that many compounds, such as alkylamines, arylamines, hydroxylamines and various heterocyclic amines, form many different *N*-glucuronides both *in-vitro* and *in-vivo* (Chiu, et al. 1998; Green, et al. 1998). These types of conjugates can be broadly categorized as aliphatic and/or aromatic amine-linked glucuronides (*N*-glucuronide) and quaternary ammonium-linked glucuronides (N^+-glucuronide). In contrast to the UGT1A family, the UGT2B enzymes are primarily responsible for the metabolism of steroids, except for UGT2B7 that has been shown to metabolize many different drugs (Radominska-Pandya, et al. 2001).

Most UGT1A proteins are expressed predominantly in the liver, but they have been also found in several extra-hepatic tissues. For example, UGT1A1, 1A3, 1A4, 1A6 and 1A9 are highly abundant in the liver, whereas UGT1A7, 1A8 and 1A10 are found

exclusively in extra-hepatic tissues such as gastric, colon and biliary tissue, respectively (Strassburg, et al. 1997). Identification of individual UGTs responsible for the metabolism of a particular drug is important for predicting the major phase II elimination route of the drug in humans.

A tricyclic indenopyrazole compound, 6,7-(dimethoxy-2,4-dihydroindeno[1,2-c] pyrazol-3-yl)-(3-fluoro-phenyl)-amine (JNJ-10198409, Figure 1), was discovered as a potent inhibitor of platelet-derived growth factor receptor (PDGFr) tyrosine kinase (Ho, et al., 2005). Over-expression of PDGF and its receptors have been implicated as drivers of tumor cell proliferation in some cancers. Anti-cancer drugs such as paclitaxel normally act as anti-proliferative agents that inhibit tumor cell growth directly (Inoue et al., 2000). During the past decade, the anti-angiogenesis agents blocking the formation of neo-vasculature in a tumor *in situ* have shown great promise as cancer drugs (Li, 2004; Bocci et al., 2004). JNJ-10198409 represents a novel anticancer agent that, as a single chemical entity, has both anti-angiogenic and tumor cell anti-proliferative activities (Tuman et al., 2004; Mei, et al., 2004; D'Andrea, et al. 2005).

JNJ-10198409 contains a pyrazole ring and an aniline, which are the potential functional groups for *N*-glucuronidation. Although the pyrazole ring is a common structural moiety, *N*-glucuronidation at the nitrogens on the pyrazole has not been documented in the literature. Therefore, it was of interest to investigate the glucuronidation of JNJ-10198409. More importantly, information about glucuronidation would be valuable for both evaluating potential drug-drug interactions and predicting the drug metabolism fate in humans.

In the present study, *in-vitro N*-glucuronidation was characterized as the major metabolic pathway of JNJ-10198409 by metabolic profiling, liquid chromatography mass spectrometry (LC/MS/MS) and nuclear magnetic resonance (NMR) analyses. Furthermore, UGT enzymes that are responsible for formation of *N*-glucuronides were characterized by using human cDNA-expressed UGTs and by enzyme kinetic analyses.

Materials and Methods

Reagents

Liver microsomes derived from rat, monkey and human tissues were obtained from Gentest Corp. (Woburn, MA). Human and monkey liver microsomes were prepared from livers of mixed gender, whereas rat liver microsomes were prepared from male animals. Microsomal protein content was previously determined by the supplier (Gentest Corp.). *Supersomes*™ containing individual UDP-glucuronosyltransferases (UGTs) were derived from baculovirus insect cells transfected with specific human UGT cDNAs. No detectable human P450 activities were found in the *Supersomes*™ preparations. JNJ-10198409, a proprietary compound, was internally synthesized at Johnson & Johnson Pharmaceutical Research & Development LLC (Ho, et al. 2005). Other reagents were purchased from Sigma (St. Louis, MO), which included alamethicin, UDPGA, *E. coli* β-glucuronidase, propofol, β-nicotinamide adenine dinucleotide phosphate ($NADP^+$), glucose-6-phosphate and glucose-6-phosphate dehydrogenase. All HPLC and NMR solvents were obtained from standard vendors.

Oxidative Metabolism of JNJ-10198409 in Liver Microsomes

All microsomal incubations were performed at 37°C in a water bath. JNJ-10198409 was separately mixed with human, monkey or rat liver microsomal protein in

50 mM phosphate buffer (pH 7.4). After a 5-min preincubation at 37^{o}C, reactions were initiated by the addition of a NADPH-generating system to give a final volume of 1.0 ml. The final reaction mixture contained 10 μM of JNJ-10198409, 1 mg/ml microsomal protein, 1.3 mM $NADP^{+}$, 3.3 mM glucose-6-phosphate, 0.4 U/ml glucose-6-phosphate dehydrogenase and 3.3 mM magnesium chloride. After a 60-min incubation, reactions were terminated by the addition of 250 μL of acetonitrile. Samples were centrifuged at 10000 g for 10 min to pellet the precipitated protein, and supernatants were subjected to LC-MS/MS analysis of oxidative metabolites formed by cytochrome P450s (CYPs).

Glucuronidation of JNJ-10198409 in Liver Microsomes

JNJ-10198409 was separately mixed with human, monkey or rat liver microsomal protein in 50 mM Tris buffer (pH 7.4) supplemented with alamethicin in aqueous solution (stock solution 1 mg/ml). After a 5-min preincubation at 37^{o}C, reactions were initiated by the addition of UDPGA to give a final volume of 0.5 mL. The final reaction mixture contained 2 mM UDPGA, 25 μg/ml alamethicin, JNJ-10198409 and microsomal protein at desired concentrations. After incubation for designated times, reactions were terminated by the addition of 250 μL of acetonitrile. Samples were centrifuged at 10000 g for 10 min to pellet the precipitated protein, and supernatants were subjected to LC-MS/MS for direct analysis of glucuronides.

Incubations of Glucuronides with β-Glucuronidase

Glucuronides were first generated by the *in-vitro* incubation with rat liver microsomes as described above. The total volume of incubation was 1 ml. After centrifugation, the supernatant was transferred to a 1.5-ml tube, and the sample was

DMD Fast Forward. Published on February 2, 2006 as DOI: 10.1124/dmd.106.009274
This article has not been copyedited and formatted. The final version may differ from this version.

concentrated to approximately 100 µl in a spin-vacuum drier. A total volume of 900 µl water was added to the concentrated sample, and the reconstituted sample was subsequently divided into three fresh tubes. One tube was stored at –80^{o}C as a control. The second tube was incubated with β-glucuronidase (500 U/ml) for 30 min at 37^{o}C, and then was stored at –80^{o}C. The third tube was remained at room temperature for 6 hrs. Finally, all three samples were analyzed for glucuronides using LC-MS/MS as described below.

Isolation of Glucuronides

A pilot study was first conducted with ovine liver microsomes, and results confirmed that JNJ-10198409 formed three glucuronides identical to those formed in rat and human liver microsomes. In order to be cost-effective, a large-scale incubation was performed using ovine liver microsomal UDP-glucuronyl-transferase and UDP-glucuronate using a literature procedure (Kren et al., 2000; Hubl et al., 2001). The reaction mixture contained ovine liver microsomal protein (2 mg/ml), UDPGA (50 mM) and DTT (0.16 mg/ml) in 200 mM Tris buffer (pH 8.0) containing 6 mM $CaCl_2$. The reaction was started by gradually adding JNJ-10198409 in DMSO to the reaction mixture. Incubation was performed for 24 hrs in a water bath set at 35°C. After centrifugation, the supernatant was applied to a 3.5x20 cm column of Merck LiChroprep RP-18 silica that was pre-equilibrated with 5% methanol supplemented with 0.025% ammonium trifluoroacetate. After washing with 100 ml of 5% methanol, a gradient of 5-65% methanol was applied over 40 min. Fractions containing glucuronides were collected and pooled. Preparation was repeated many times to accumulate enough material. Solvents were removed by rotary evaporation. The resulting solid from the RP-

DMD Fast Forward. Published on February 2, 2006 as DOI: 10.1124/dmd.106.009274
This article has not been copyedited and formatted. The final version may differ from this version.

18 column was dissolved in Milli-Q water and purified by preparative HPLC using a 250x21.4cm Jupiter C-18 column (15μ, 100Å) (Phenomenex, Torrance, CA) and running a gradient of 2.5-50% methanol over 45 min.. Fractions containing individual glucuronides were collected and dried by rotary evaporation to obtain solid materials. Purity of isomeric glucuronides was checked by LC-MS/MS and NMR analysis.

Glucuronidation of JNJ-10198409 by cDNA-expressed UGTs

Glucuronide formation rates were determined using *Supersomes*™ containing cDNA expressed individual UGTs (UGT1A1, 1A2, 1A3, 1A4, 1A6, 1A7, 1A8, 1A9, 2B4, 2B7, 2B15 and 2B17). All incubations were performed in triplicate in a 96-well plate at 37°C in a water bath. JNJ-10198409 at desired concentrations was pre-incubated for 5 min with *Supersomal* protein (0.25 mg/ml) in 50 mM Tris buffer (pH 7.4, 3.5 mM $MgCl_2$). The conjugation reaction was initiated by the addition of 2 mM UDPGA. At designated incubation times, the reaction was terminated by the addition of ice-cold acetonitrile. Samples were centrifuged at 10000 g for 20 min to pellet the precipitated protein, and the resulting supernatants were transferred to HPLC vials for LC-MS/MS analysis of formed glucuronides.

Determination of the Kinetic Constants of Glucuronides

The kinetic constants of K_m and V_{max} were determined for two glucuronides (designated Glu-A and B) by incubating JNJ10198409 at various concentrations (0, 0.13, 0.4, 1.2, 3.7, 11.1, 33.3 and 100 μM) with either pooled human liver microsomes (0.5 mg/ml) or *Supersomes*™ (0.25 mg/ml) containing individual UGTs under the same conditions described above. Three replicates of incubation were performed at each drug concentration. The data were analyzed by iterative nonlinear least squares regression

DMD Fast Forward. Published on February 2, 2006 as DOI: 10.1124/dmd.106.009274
This article has not been copyedited and formatted. The final version may differ from this version.

analysis using Prism 3.5 (GraphPad Software Inc., San Diego, CA), fitting the data to the Michaelis-Menten equation.

Propofol Inhibition of JNJ-10198409 Glucuronidation

The effect of propofol, a specific inhibitor of UGT1A9, on JNJ-10198409 glucuronidation was investigated using pooled human liver microsomes. Propofol (100 μM) was added to incubation mixtures containing JNJ-10198409 at various concentrations to investigate the involvement of UGT1A9. The microsomal protein concentration was 0.25 mg/ml, and the incubation time was 10 min. Formed glucuronides were analyzed by LC-MS/MS as described below. Glucuronidation rates were expressed relative to the control (no inhibitor).

LC-MS/MS Analysis of Glucuronides

LC-MS/MS analyses were performed on a Micromass (Manchester, UK) *Quattro Micro* triple quadrupole mass spectrometer interfaced to an Agilent 1100 HPLC system. LC-MS/MS analyses were conducted using electrospray ionization (ESI) under either the positive or negative ion mode. The capillary voltage was 3.1 kV, and the cone voltage was set at 20 V to minimize in-source dissociation of glucuronides (Yan et al., 2003a). The source temperature was set at 120 ^{o}C, and the desolvation temperature was 300 ^{o}C. The collision gas was argon.

An Agilent Zorbax SB C18 column (2.1 x 100 mm) was used for the chromatographic separations. The starting mobile phase consisted of 95% water (0.5% acetic acid), and glucuronides were eluted using a linear gradient of 95% water to 95% acetonitrile over 7 min at a flow rate of 0.3 ml/min. At 7 min, the column was flushed with 95% acetonitrile for 2 min before re-equilibration at initial conditions for 2 min.

DMD Fast Forward. Published on February 2, 2006 as DOI: 10.1124/dmd.106.009274
This article has not been copyedited and formatted. The final version may differ from this version.

During the run, the divert valve was activated to divert the HPLC eluant to waste for the first minute of elution, and then switched to the mass spectrometer for analysis. LC-MS/MS analysis was carried out on 10-µl aliquots from incubations. To obtain a tandem spectrum, the mass spectrometer was operated in the product ion scan mode. For quantification of glucuronides, multiple reaction monitoring (MRM) mode was ultilized to detect transitions at *m/z* 502→326.

For detecting glucuronides by ESI in the negative mode, 2 mM ammonium acetate was added to aqueous mobile phase. The same LC gradient profile was utilized for chromatographic separation. The MS transition *m/z* 500→324 was utilized. Data were processed using the *Masslynx v3.5* software from Micromass (Manchester, UK).

NMR Analysis of Glucuronides

One dimensional (1D) and two dimensional (2D) NMR spectra were obtained on a Bruker-Biospin, Inc DRX-500 MHz or a DMX-600 MHz spectrometer using XWINNMR acquisition and processing software. The spectra were collected using a z-gradient inverse broadband probe (500 MHz) or a triple tuned three-axis gradient probe (600 MHz) at various temperatures. Typical 1D proton (^{1}H) NMR spectra were obtained using standard pulse and acquisition sequences. Typical 1D carbon (^{13}C) NMR (150.917 MHz) spectra were obtained using standard sequences with composite pulse decoupling techniques. The 2D homonuclear correlated spectroscopy gradient (g-COSY) experiment was used to obtain ^{1}H-^{1}H coupling correlations. A mixing pulse of 90 degrees was used and one scan was measured for 128 values of t_1 to give a total matrix of 128 X 2048 complex points with a spectral width of 2670.940 Hz. The FID was multiplied with a sine-bell function in both dimensions and symmetrized about the diagonal. The 2D

nuclear Overhauser enhancement spectroscopy gradient (g-NOESY) experiment was used to obtain ^{1}H-^{1}H spatial correlations. A mixing time of 500 μs was used and 64 scans were measured for 256 values of t_1 to give a total matrix of 256 X 2048 complex points with a spectral width of 4370.629 Hz. The FID was multiplied with a squared sine-bell in both dimensions. The 2D heteronuclear multiple bond correlated spectroscopy gradient (g-HMBC) experiment was used to obtain long-range ^{1}H-^{13}C couplings. The delay was optimized for 8 Hz couplings. A total of 2048 scans were measured for 128 values of t_1 to give a total data matrix of 128 X 2048 complex points. The carbon F_1 spectral width was 21250 Hz and the proton F_2 spectral width was 4370.629 Hz. Data were processed using squared sine-bell function in both dimensions. The compounds were dissolved in either dimethyl sulfoxide-d_6 (DMSO-d_6) or methanol-d_4 (CD_3OD) in 5 mm tubes. The chemical shifts (δ) measured in parts-per-million (ppm) were referenced internally to DMSO (δ_H 2.50 ppm and δ_C 39.5 ppm) or CH_3OH (δ_H 3.30 ppm and δ_C 49.15 ppm) (Table 1 & 2).

Results

In-vitro Metabolism of JNJ-10198409

JNJ-10198409 was slowly metabolized in NADPH-fortified liver microsomes derived from human, rat and monkey tissues. Several oxidative metabolites were identified at low levels in microsomal incubations, which included *O*-demethylation metabolites and *N*-oxides at the secondary aromatic nitrogen atoms (data not shown). In contrast, JNJ-10198409 was rapidly metabolized in the presence of UDPGA in liver microsomes that were pre-treated with alamethicin, a pore-forming peptide used to fully activate latent UGTs (Yan et al., 2003b; Fisher et al., 2000). In rat liver microsomes, LC-MS/MS with ESI analyses detected three isomeric metabolites (MH^+ at m/z 502),

designated as Glu-A (RT 5.3 min), Glu-B (RT 5.6 min) and Glu-C (RT 4.8 min), respectively (Figure 2A). In incubations with liver microsomes derived from monkey, Glu-B was more abundant than Glu-A (Figure 2B); Glu-A and Glu-B were at a comparable level in human liver microsomes (Figure 2C). The level of Glu-C was not detectable in either human or monkey liver microsomes.

Tandem MS spectra of all three components are shown in Figure 3. The predominant product ion appeared at *m/z* 326 for all three metabolites. The cations at *m/z* 326 $(M-176)^+$ likely resulted from the cleavage of the glycosidic bond with transfer of a proton from the glucuronic acid moiety to the aglycone. The Glu-A MS spectrum (3A) also contained prominent product ions at *m/z* at 350 and 368. All three glucuronides were detected by ESI-MS at *m/z* 500 in the negative mode, although signal-to-noise ratios were significantly lower compared to that observed in the positive mode (data not shown).

The pyrazole heterocycle ring system can exist in two tautomeric forms (Figure 1), which suggests that, in addition to the formation of *N*-glucuronides, quaternary ammonium-linked glucuronide metabolites (i.e., N^+-glucuronides) could be also derived from JNJ-10198409. Based on previous 2D NMR experiments, it was concluded that JNJ-10198409 existed primarily as the pyrazole N(1)H tautomer (Figure 1; form-II) (Ho, et al., 2005). The NMR study also demonstrated that there was significant hindered rotation about the pyrazole-N(H)-phenyl ring systems. From a structural standpoint, if JNJ-10198409 is primarily in form-II, it possesses two secondary amines that could result in the formation of *N*-glucuronides. Glucuronidation of the tertiary amine in form-II would result in the formation of an N^+-glucuronide. Since the equilibrium ratio of the tautomeric forms of JNJ10198409 are dependent on environmental factors such as pH,

temperature, and median ionic strength, it is likely that form-I will also be present under our *in-vitro* experimental conditions. In this case, instead of N^+-glucuronidation at the tertiary amine N(2) in form-II, glucuronidation of the secondary amine in form-I would result in the formation of a *N*-glucuronide.

In the positive ESI mode, the two types of *N*-glucuronide metabolites cannot be distinguished from each other. For example, glucuronidation of JNJ-10148409 at a secondary amine would result in the formation of metabolites with molecular weight of 501 Da. Under positive ESI conditions, molecular ions at *m/z* 502 would be detected. Glucuronidation of JNJ-10148409 at a tertiary amine would result in the formation of positively charged metabolites with a molecular weight of 502 Da. Under positive ESI conditions, cations at *m/z* 502 would be detected. Thus, under positive ESI conditions both types of *N*-glucuronides would appear at *m/z* 502. The two types of *N*-glucuronide metabolites can be distinguished by LC-ESI-MS in the negative mode. Glucuronidation of JNJ-10148409 at a secondary amine would result in the formation of metabolites with a molecular weight of 501 Da, which appear as molecular ions at *m/z* 500 (M-1) in the negative ESI mode. Since the N^+-glucuronide contains a positive charge, it would not be detected in the negative mode (Vashishtha et al., 2002). Our results indicated that all three glucuronides were formed at secondary amines. Definitive identification of individual glucuronides could not be made solely by MS/MS analysis.

NMR Identification of Glucuronides

In order to determine the structures of individual glucuronides by NMR, Glu-A, Glu-B and Glu-C were purified from large-scale ovine liver microsomal incubations by semipreparative HPLC. The purified conjugates had HPLC retention times and MS/MS

DMD Fast Forward. Published on February 2, 2006 as DOI: 10.1124/dmd.106.009274
This article has not been copyedited and formatted. The final version may differ from this version.

characteristic cations identical to those generated in rat, monkey and human microsomal incubations.

The structure of the three glucuronides isolated from ovine liver microsomal incubations are shown in Figure 4. The proton (^{1}H) NMR and carbon (^{13}C) chemical shift assignments of JNJ-10148409 and its three corresponding *N*-glucuronides are shown in Tables 1 and 2, respectively. A representative proton NMR spectrum (i.e., Glu-B) is shown in Figure 5. The proton resonance assignments were based on expected proton coupling relationships, chemical shifts, g-COSY and g-NOESY experiments. For the sugar moiety, the coupling constant of the H1' proton (i.e., $J_{1',2'} = 7.8$ Hz) was indicative of β-glucuronide stereochemistry (Smith et al., 1986). The carbon resonance assignments were based on ^{1}H-^{13}C g-HMBC experiments.

The structural assignments of the three N-glucuronides are based on a series of 2D NMR experiments involving g-NOESY (i.e., ^{1}H-^{1}H spatial correlations) and g-HMBC (i.e., ^{1}H-^{13}C long range couplings) experiments. The structural assignment of Glu-A was based primarily on the observation of a close proximity ^{1}H-^{1}H spatial relationship between the H1' proton on the glucuronic acid moiety and the protons H15/H19 on the phenyl ring. In addition, the HMBC experiment indicated that there was a three bond coupling between H1' and the quaternary carbon C14 on the phenyl ring. (i.e., H1'-N13-C14). These results are unique to the Glu-A structure. The structural assignment of Glu-B was based on the observation of a ^{1}H-^{1}H spatial relationship between the H1' proton on the glucuronic acid moiety and the H10 aromatic proton on the indenopyrazole ring. The HMBC experiment indicated that there was a three bond coupling between H1' and the quaternary carbon C12 on the indenopyrazole ring. (i.e.,

H1'-N1-C12). These results are distinctive to the Glu-B structure. The structural assignment of Glu-C was based the HMBC experiment which indicated that there was a three bond coupling between H1' and the quaternary carbon C3 on the pyrazole ring. (i.e., H1'-N2-C3).

Degradation of *N*-Glucuronides of JNJ-10198409 by β-Glucuronidase.

Three glucuronides were generated in microsomal incubations with rat liver microsomes. Glucuronides formed in incubation mixtures were treated with β-glucuronidase. It was found that both Glu-A and Glu-C completely disappeared after treatment with β-glucuronidase. Under the same conditions, Glu-B remained intact after a 30-min incubation at 37 ^{o}C (data not shown). In absence of β-glucuronidase, both Glu-A and Glu-C underwent slow degradation; after sitting for 6 hrs at room temperature, 67% and 72% of Glu-A and Glu-C remained respectively, but no significant degradation was observed for Glu-B under the same conditions. It was also found that purified Glu-A and Glu-C underwent degradation, and degradation was not inhibited by saccharolactone.

Kinetics of Formation of Glu-A and Glu-B in HLM.

Due to clinical relevance in human, kinetics studies were undertaken focused on the formation of Glu-A and Glu-B in human liver microsomes. Initial velocity conditions were established, which were linear with respect to both protein concentration and incubation time. Primary data also indicated the formation rates of Glu-A and Glu-B were linear with incubation time up to 25 min and with microsomal protein concentration up to 0.75 mg/ml. Therefore, kinetic studies of glucuronidation were carried out at a protein concentration of 0.5 mg/ml over 10 min. Incubations of JNJ-10198409 over the concentration range of 1 to 100 μM with pooled human liver microsomes resulted in the

DMD Fast Forward. Published on February 2, 2006 as DOI: 10.1124/dmd.106.009274
This article has not been copyedited and formatted. The final version may differ from this version.

concentration-dependent formation of Glu-A and Glu-B. Kinetic analyses showed that formation of Glu-A and Glu-B exhibited atypical kinetics. As shown in the Eadie-Hofster transformation plot (Figure 6), a non-linear plot was observed for both GluA and Glu-B. A biphasic Michaelis-Menten model was applied to estimate the apparent kinetic parameters (K_{m1} and V_{max1}) of the high affinity binding, with the assumption that two enzymes catalyzed the glucuronidation (see Table 3). The calculated intrinsic clearances (V_{max1}/K_{m1}) for the formation of Glu-A and Glu-B were 2002 nmole min^{-1} mg^{-1}/μM and 2403 nmole min^{-1} mg^{-1}/μM, respectively. Because of low solubility, data points at high substrate concentrations were too limited to estimate Michaelis-Menten kinetic parameters (K_{m2} and V_{max2}) of the low affinity binding.

Glucuronide Formation in Recombinant UGT Enzymes.

The formation of Glu-A and Glu-B was investigated in microsomes derived from baculovirus-infected insect cells (*Supersomes*) that expressed single recombinant human UGT enzymes. As shown in Table 4, at 100 μM of JNJ-10198409, UGT1A9, 1A8 and 1A7 were the most active isozymes catalyzing formation of Glu-A with glucuronidation rates of 1869 nmole min^{-1} mg^{-1}, 1361 nmole min^{-1} mg^{-1} and 1344 nmole min^{-1} mg^{-1}, respectively, which is followed by UGT1A4 with a glucuronidation rate of 576 nmole min^{-1} mg^{-1}. UGT1A1, 1A10 and 1A3 demonstrated lower glucuronidation with reaction rates of 146 nmole min^{-1} mg^{-1}, 98 nmole min^{-1} mg^{-1} and 41 nmole min^{-1} mg^{-1}, respectively. For Glu-B formation, UGT1A9 was the most active enzyme with a glucuronidation rate of 2384 nmole min^{-1} mg^{-1}, which is followed by UGT1A3 (1003 nmole min^{-1} mg^{-1}), UGT1A7 (834 nmole min^{-1} mg^{-1}) and UGT1A4 (816 nmole min^{-1} mg^{-1}). Although UGT1A1 and 1A8 also catalyzed formation of Glu-B, the rate was very low

(UGT1A1, 155 nmole min^{-1} mg^{-1}; UGT1A8, 144 nmole min^{-1} mg^{-1}) compared to the other isoforms. In contrast to UGT1A enzymes, UGT2B members including UGT2B4, 2B7, 2B15 and 2B17 were all inactive in the glucuronidation of JNJ-10198409.

Kinetics of Glu-A and Glu-B by Individual UGTs.

Kinetic studies were then focused on the formation of Glu-A and Glu-B by the most active UGT enzymes including UGT1A3, UGT1A4, 1A7, 1A8 and 1A9. Incubation conditions were initially optimized using various protein concentrations and for various times. It was found that formation of Glu-A and Glu-B was linear at 0.5 mg/ml protein within 30 min for UGT1A4, 1A7, 1A8 and 1A9. Formation of Glu-A by UGT1A3 was not significant, and kinetic parameters were not determined. For other tested UGT enzymes, incubations of JNJ-10198409 over the concentration range of 1 to 100 μM with individual UGTs resulted in a concentration-dependent formation of Glu-A and Glu-B. Kinetic analyses indicated that formation of Glu-A and Glu-B by all those UGT enzymes followed classic Michaelis-Menten kinetics with a correlation coefficient (r^2) in the range of 0.95-0.99, suggesting all enzymes have a single binding site. All kinetic constants are given in Table 5.

Propofol Inhibition of JNJ-10198409 Glucuronidation.

UGT1A9 was shown to be the most active enzyme catalyzing the glucuronidation of JNJ-10198409. To determine the relative contribution of UGT1A9 to both Glu-A and Glu-B formation in human liver microsomes, the effect of propofol, a selective UGT1A9 competitive inhibitor (Girard, et al. 2004), on the effect of JNJ-10198409 glucuronidation was determined (Table 6). At a lower drug concentration (1 μM), propofol effectively inhibited formation of both Glu-A and Glu-B. At higher drug concentrations (5 and 25

μM), propofol showed little inhibition of Glu-A and B formation in human liver microsomes. Other UGT inhibitors have not been proven to be highly specific; therefore, inhibition activity towards formation of Glu-A and B were not investigated in this study.

Discussion

N-glucuronidation plays a significant role in the metabolic elimination of many aliphatic tertiary amine-containing therapeutic agents (Green, et al. 1998). Initial results from our *in-vitro* studies suggested that glucuronidation was the major elimination pathway for JNJ10198409. In rat liver microsomal incubations, three *N*-glucuronides, Glu-A, B and C, were detected by LC-MS/MS. Only Glu-A and B were found in monkey and human liver microsomes. All three glucuronides were detected in rat plasma, whereas Glu-A and Glu-B were predominant glucuronides in plasma samples collected from monkeys (unpublished data). Thus, the *in-vitro* and *in-vivo* results were consistent. None of those oxidative metabolites identified in microsomal incubations were detected in either rat or monkey samples.

JNJ-10198409 has three nitrogen atoms. NMR analysis of isolated glucuronides indicated that all three conjugates are secondary *N*-glucuronides, which appeared to be consistent with the tautomerization of JNJ-10198409 (Figure 1). Many aromatic heterocyclic amines have been reported to form *N*-glucuronides (Chiu, et al., 1998), which include imidazole (Pahernik, et al., 1995), pyridine (Sakamoto, et al., 1993), tetrazole (Sterns et al., 1992; Huskey et al., 1994) and triazoles (Huskey et al., 1994). Glu-B appears to be the first documented example showing that the glucuronic acid moiety is linked to the pyrazole ring. Also, the results indicated that both aromatic nitrogen atoms of the pyrazole ring form *N*-glucuronides.

Species differences in glucuronidation of JNJ-10198409 were observed in the present study. In rat, three glucuronides were detected, and Glu-A is the most abundant conjugate followed by Glu-C and Glu-B. In contrast, only two glucuronides, Glu-B and Glu-A, were formed in incubations with monkey and human liver microsomes. Similar species differences in *N*-glucuronidation were observed in rat and monkey dosed with JNJ-10198409. Previous studies have shown that *N*-glucuronidation exhibited species differences *in-vitro* and *in-vivo*, but species differences are generally less striking for compounds forming non-quaternary *N*-conjugates (Chiu, et al. 1998; Kaji et al., 2005).

Stability differences were observed for the three glucuronides. Both Glu-A and Glu-C are hydrolyzed by β-glucuronidase, and underwent slow degradation at neutral pH. In contrast, Glu-B was resistant to hydrolysis by bacterial β-glucuronidases and did not decompose under mild conditions. Previous studies have shown that *N*-glucuronide metabolites of the primary/secondary amines and *N*-glucuronides of *N*-hydroxylated amines were hydrolyzed to the parent compounds and glucuronic acid under mild or acidic conditions (Mohri et al., 2001; Kadlubar et al., 1977), while the quaternary-ammonium glucuronides were hydrolyzed under basic conditions (Dulik et al., 1987; Kowalczyk et al., 2000). Among the several quaternary-ammonium glucuronides tested for stability in the presence of β-glucuronidase from bovine liver and *E. coli*, only bacterial enzyme hydrolyzed all *N*-glucuronides (Kowalczyk et al., 2000). It is interesting to note that Glu-B showed distinct stability compared to Glu-C and Glu-A, two isomeric glucuronides.

Kinetic studies revealed that *N*-glucuronidation of JNJ-10198409 in human liver microsomes did not follow classic Michaelis-Menten kinetics. A likely explanation for

the non-classic Michaelis-Menten kinetics is the involvement of multiple UGT enzymes in glucuronidation of JNJ-10198409 in human liver microsomes. This argument is largely supported by the observation that several recombinant UGT1A enzymes (e.g. UGT1A9, 1A8 and 1A7) catalyzed glucuronidation of JNJ-10198409. In addition, kinetic analyses indicated that all glucuronidation reactions catalyzed by individual recombinant UGT enzymes followed classic Michaelis-Menten kinetics. At present, it is not clear whether incomplete removal of glucuronidation latency in human liver microsomes may also lead to atypical Michaelis-Menten kinetics of glucuronidation of JNJ-10198409. Atypical Michaelis-Menten kinetics has been previously reported in both glucuronidation (Watanabe, et al. 2002; Stone, et al. 2003; Kirkwood, et al. 1998) and biotransformation mediated by CYPs (Hutzler, et al. 2002; Ekins, et al. 1998).

Identification of the specific UGTs for *N*-glucuronidation of JNJ10198409 would allow future investigation of potential drug-drug interaction as well as possible polymorphism in *N*-glucuronidation of JNJ10198409. Although definitive identification of UGT isozymes is difficult at present, largely due to lack of enzyme-specific substrates and inhibitors for correlation and selective inhibition studies, characterization of UGT isoforms responsible for a glucuronidation reaction has become possible because of availability of cDNA expressed UGTs. Several UGT1A enzymes such as UGT1A4, UGT1A7, UGT1A8 and UGT1A9 were all active in catalyzing the formation of both Glu-A and Glu-B, which is probably due to efficient binding of JNJ10198409 to those UGT1A enzymes. One should note that observations in individual recombinant UGTs may not simply be relevant to the liver tissue since it has been known that UGT activity and substrate specificity can change via heterodimerization with other isozymes.

It is interesting to note that, even though the pyrazole ring could undergo tautomerization (Figure 1), glucuronidation of the pyrazole moiety by human UGT1A enzymes exclusively occurred at the *N*-1 position, which could be explained by the difference in the orientation of individual nitrogen atoms within the active sites of UGT1A. An alternative explanation is that the steric effect of the fluoro-phenyl-amine substitutent on the *N*-2 position of the pyrazole ring. However, this hypothesis could not explain the glucuronidation of the aliphatic amine that is also sterically hindered by the fluoro-phenyl moiety. Because of its unique difference in *N*-glucuronidation, it is our speculation that JNJ-10198409 could potentially serve as a model substrate for probing the structure-activity relationship of UGT1A enzymes such as UGT1A9.

Additionally, present results appear to suggest that UGT1A9 may play a more important role than other isoforms in hepatic glucurnidation of JNJ-10198409 at low drug concentrations (< 1 μM). This conclusion is supported by the following two observations. First, UGT1A9 is the most active enzyme catalyzing glucuronidation of JNJ-10198409 in human liver microsomes; second, at low drug concentrations, formation of Glu-A and Glu-B was effectively inhibited by the UGT1A9 selective inhibitor propofol. Inability of inhibiting glucuronidation by propofol at high drug concentrations (> 1μM) suggested that multiple enzymes were likely involved in the glucuronidation of JNJ10198409. Since UGT1A7 and 1A8, two enzymes highly expressed in extra-hepatic tissues, were also active in glucuronidation of JNJ10198409, it is likely that the first-pass phase-II metabolism may also play a significant role in the clearance of the drug. Therefore, one should not simply interpret the in-vivo relevance of the in-vitro results. Because the drug is likely to be metabolized by multiple UGT1A enzymes expressed in different tissues, it

is reasonable to speculate that neither UGT-mediated drug-drug interactions nor polymorphism of UGT genes is an obvious concern.

In conclusion, *N*-glucuronidation of JNJ10198409, a novel potential anticancer agent, was elucidated using rat, monkey and human liver microsomes. Species differences were observed; three glucuronides formed in rat, and two conjugates were detected in monkey and human liver microsomes. The Glu-B conjugate is the first documented example showing that the glucuronic acid moiety is linked to an aromatic nitrogen of the pyrazole ring. It was also found that multiple UGT enzymes are responsible for the *N*-glucuronidation of this compound in human liver microsomes.

References

Bocci G; Danesi R; Marangoni G; Fioravanti A; Boggi U; Esposito I; Fasciani A; Boschi E; Campani D; Bevilacqua G; Mosca F; Del Tacca M. (2004) Antiangiogenic versus cytotoxic therapeutic approaches to human pancreas cancer: an experimental study with a vascular endothelial growth factor receptor-2 tyrosine kinase inhibitor and gemcitabine. *Europ. J.Pharmacol.* **498**: 9-18.

Chiu SH; Huskey SW (1998) Species differences in *N*-glucuronidation. *Drug Metab. Dispos* **26**: 838-847.

D'Andrea RM; Mei MJ; Tuman WR; Galemmo AR and Johnson LD. (2005) Validation of *in vivo* pharmacodynamic action of a novel PDGF receptor tyrosine kinase inhibitor using immunohistochemistry and quantitative image analysis. *Molecular Cancer Therapeutics*. 1198-1204.

Dulik DM; Fenselau, C. (1987) Species-dependent glucuronidation of drugs by immobilized rabbit, rhesus monkey, and human UDP-glucuronyl transferases. *Drug Metab. Dispos* **15**: 473-477.

Ekins S; Ring BJ; Binkley SN; Hall SD; Wrighton SA. (1998) Autoactivation and activation of the cytochrome P450s. *Intern. J. Clin. Pharmacol. Therap.* **36**: 642-651.

Fisher MB; Campanale K; Ackermann BL; Vandenbranden M; Wrighton SA. (2000) In vitro glucuronidation using human liver microsomes and the pore-forming peptide alamethicin. *Drug Metab. Dispos* **28**: 560-566.

Girard H; Court MH; Bernard O; Fortier L-C; Villeneuve L; Hao Q; Greenblatt DJ; von Moltke, LL; Perussed L; Guillemette C. (2004) Identification of common polymorphisms in the promoter of the UGT1A9 gene: evidence that UGT1A9 protein and activity levels are strongly genetically controlled in the liver. *Pharmacogenetics* **14**: 501-515.

Green MD; Tephly TR. (1998) Glucuronidation of amine substrates by purified and expressed UDP-glucuronosyltransferase proteins. *Drug Metab. Dispos* **26**: 860-867.

Ho CY; Ludovici DW; Maharoof USM; Mei J; Sechler JL; Tuman RW; Strobel ED; Andraka L; Yen H-K; Leo G; Li J; Almond H; Lu H; DeVine A; Tominovich RM; Baker J; Emanuel S; Grunninger RH; Middleton SA; Johnson DL; Galemmo RAJ (2005) (6,7-Dimethoxy-2,4-dihydroindeno[1,2-c]pyrazol-3-yl)phenylamines: PDGF receptor tyrosine kinase inhibitors with broad anti-proliferative activity against tumor cells *J. Med. Chem.* **48**: 8163-8173

Hubl U; Stevenson DE. (2001) In vitro enzymic synthesis of mammalian liver xenobiotic metabolites catalysed by ovine liver microsomal cytochrome P450. *Enz. Microb. Technol*., **29**: 306-311.

Huskey SE; Magdalou J; Ouzzine M; Siest G; Chiu SH. (1994) *N*-glucuronidation reactions. III. Regioselectivity of *N*-glucuronidation of methylbiphenyl tetrazole, methylbiphenyl triazole, and methylbiphenyl imidazole using human and rat recombinant UDP-glucuronosyltransferases stably expressed in V79 cells. *Drug Metab. Dispos* **22**: 659-562.

Hutzler JM; Kolwankar D; Hummel MA; Tracy TS. (2002) Activation of CYP2C9-mediated metabolism by a series of dapsone analogs: Kinetics and structural requirements. *Drug Metab. Dispos* **30**: 1194-1200.

Inoue K; Slaton JW; Davis DW; Hicklin DJ; McConkey DJ; Karashima T; Radinsky R; Dinney, CPN. (2000) Treatment of human metastatic transitional cell carcinoma of the bladder in a murine model with the anti-vascular endothelial growth factor receptor monoclonal antibody DC101 and paclitaxel. *Clin. Cancer Res.* **6:** 2635-2643.

Kadlubar FF; Miller JA; Miller EC (1977) Hepatic microsomal *N*-glucuronidation and nucleic acid binding of *N*-hydroxy arylamines in relation to urinary bladder carcinogenesis. *Cancer Research,* **37**: 805-14.

Kaji H; Kume T. (2005) Characterization of afloqualone *N*-glucuronidation: Species differences and identification of human UDP-glucuronosyltransferase isoform(s). *Drug Metab. Dispos* **33**: 60-67.

King CD; Rios GR; Green MD; Tephly TR. (2000) UDP-Glucuronosyltransferases. *Cur. Drug Metab.* **1**: 143-161.

Kirkwood LC; Nation RL; Somogyi AA. (1998) Glucuronidation of dihydrocodeine by human liver microsomes and the effect of inhibitors. *Clin. Exper. Pharmacol. Physiol.* **25**: 266-270.

Kowalczyk I; Hawes EM; McKay G. (2000) Stability and enzymatic hydrolysis of quaternary ammonium-linked glucuronide metabolites of drugs with an aliphatic tertiary amine-implications for analysis. *J. Pharma. Biomed. Analysis* **22**: 803-811.

Kren V, Ulrichová J; Kosina P; Stevenson D; Sedmera P; Prikrylová, V; Halada P; Simánek V. (2000) Chemoenzymatic preparation of silybine β-glucuronides and their biological evaluation. *Drug Metab. Dispos* **28**: 1513-1517.

Kuehl GE; Murphy Sharon E. (2003) N-glucuronidation of nicotine and cotinine by human liver microsomes and heterologously expressed UDP-glucuronosyltransferases. *Drug Metab. Dispos* **31**: 1361-1368.

Li, WW. (2004) Tumor angiogenesis as a target for early intervention and cancer prevention. *Cancer Chemoprevention* **1:** 611-633.

Mackenzie P I.; Owens IS.; Burchell B; Bock KW; Bairoch A; Belanger A; Fournel-Gigleux S; Green M.; Hum, DW; Iyanagi T; Lancet D; Louisot P; Magdalou J; Chowdhury JR; Ritter JK; Schachter H; Tephly TR; Tipton KF; Nebert DW. (1997) The UDP glycosyltransferase gene superfamily: recommended nomenclature update based on evolutionary divergence. *Pharmacogenetics*, **7**: 255-269.

Mei, J.; Tuman, R.W.; Ho, C.; Galemmo, R.; Sechler, J.; Devine, A.; Lu, H.; Garrabrant, T.; Ludovici, D.; Strobel, E.; Maharoof, U.; Tominovich, R.; Voina, S.; Emanuel, S.; Gruninger, R.; Brunmark, A.; Johnson, D.L., A Novel PDGF Receptor Kinase Inhibitor

with Dual Anti-Angiogenesis and Tumor Cell Anti-Proliferative Activity. *AACR Annual Meeting*, Orlando, FL, March 27-31, 2004, Abstract #3990; *Proceedings* **2004** (45) 921.

Mohri K; Uesawa Y; Uesugi T (2001) Metabolism of bucolome in rats. Stability and biliary excretion of bucolome *N*-glucuronide. *J. Chromatography*. B, **759**: 153-159.

Pahernik SA; Schmid J; Sauter T; Schildberg FW; Koebe HG (1995) Metabolism of pimobendan in long-term human hepatocyte culture: in vivo-in vitro comparison. *Xenobiotica*, **25**: 811-823.

Radominska-Pandya A; Little JM; Czernik PJ. (2001) Human UDP-glucuronosyltransferase 2B7. *Cur. Drug Metab.* 2: 283-298.

Sakamoto K; Nakamura Y. (1993) Urinary metabolites of pinacidil. II. Species difference in the metabolism of pinacidil. *Xenobiotica*, **23**: 649-656.

Smith CP; Benet LZ. (1986) Characterization of the isomeric esters of zomepirac glucuronide by proton NMR. *Drug Metab. Dispos.*, **14**: 503-505.

Stearns RA; Miller RR; Doss GA; Chakravarty PK; Rosegay A; Gatto G J; Chiu S H (1992) The metabolism of DuP 753, a nonpeptide angiotensin II receptor antagonist, by rat, monkey, and human liver slices. *Drug Metab. Dispos* **20**: 281-287.

Stone AN; MacKenzie PI; Galetin A; Houston BJ; Miners JO. (2003) Isoform selectivity and kinetics of morphine 3- and 6-glucuronidation by human UDP-glucuronosyltransferases: Evidence for atypical glucuronidation kinetics by UGT2B7. *Drug Metab. Dispos* **31**: 1086-1089.

Strassburg CP; Oldhafer K; Manns MP; Tukey RH. (1997) Differential expression of the UGT1A locus in human liver, biliary, and gastric tissue: identification of UGT1A7 and UGT1A10 transcripts in extrahepatic tissue. *Mol. Pharmacol.* **52**: 212-220.

Tuman, R.W.; Mei, J.; Ho, C.; Galemmo, R.; Ludovici, D.; Baker, J.; Burns, C.; Devine, A.; Maharoof, U.; Sechler, J.; Strobel, E.; Tominovich, R.; Skrzat, S.; Voina, S; Johnson,

D.L., Discovery of A Novel, Dual Mechanism Anti-Angiogenic and Anti-Proliferative Agent with Oral Anti-Tumor Activity. *AACR Annual Meeting*, Orlando, FL, March 27-31, 2004, Abstract #4558; *Proceedings* **2004** (45) 921

Vashishtha, SC; Hawes EM; McCann DJ; Ghosheh O; Hogg L. (2002) Quaternary ammonium-linked glucuronidation of 1-substituted imidazoles by liver microsomes: interspecies differences and structure-metabolism relationships. *Drug Metab. Dispos* **30**: 1070-1076.

Watanabe Y; Nakajima M; Yokoi T. (2002) Troglitazone glucuronidation in human liver and intestine microsomes: high catalytic activity of UGT1A8 and UGT1A10. *Drug Metab. Dispos* **30**:1462-1469.

Yan Z; Caldwell GW; Jones WJ; Masucci JA. (2003a) Cone voltage induced in-source dissociation of glucuronides in electrospray and implications in biological analyses. *Rapid Comm. in Mass Spectr.* **17**: 1433-1442.

Yan Z; Caldwell GW. (2003b) Metabolic assessment in liver microsomes by co-activating cytochrome P450s and UDP-glycosyltransferases. *Europ. J. Drug Metab. Pharmacokin.* **28**: 223-232.

Legends

Figure 1. Structure and numbering scheme of JNJ-10198409. Form II is the preferred tautomer.

Figure 2. Glucuronides formed by JNJ-10198409 in incubations with liver microsomes derived from rat (a), monkey (b) and human (c) tissues.

Figure 3. Tandem MS spectra of three glucuronides: Glu-A, Glu-B and Glu-C.

Figure 4. *N*-glucuronides of JNJ-10198409. *N*-glucuronidation occurs at the secondary phenyl amine (13) (Glu-A), at the aromatic nitrogen (1) on the pyrazole ring (Glu-B), and at the aromatic nitrogen (2) on the pyrazole ring (Glu-C).

Figure 5. Proton NMR spectra of glucuronides of Glu-B in CD_3OD at 300K. The protons were assigned using a series of COSY and NOESY experiments. See Figure 4 for numbering scheme.

Figure 6. Eadie-Hofstee plots for the formation of Glu-A (a) and Glu-B (b).

DMD Fast Forward. Published on February 2, 2006 as DOI: 10.1124/dmd.106.009274
This article has not been copyedited and formatted. The final version may differ from this version.

Table 1: *Proton (^{1}H) NMR chemical shift assignment (ppm) of JNJ-10148409 and its glucuronides (temperature 300K)*

Proton Number[a]	JNJ10148409[b] DMSO-d_6 (ppm)[c]	Glu-A DMSO-d_6 (ppm)[c]	Glu-B CD_3OD (ppm)[c]	Glu-C (ppm)[c]	
				DMSO-d_6	CD_3OD
NH_1	12.10 s	n.d.	n.d.	n.d.	n.d.
NH_{13}	8.75 s	n.d.	n.d.	8.47 s	n.d.
H15	7.38 d	6.74 bs	7.19 bs	6.62 d	6.67 d
H7	7.23 s	7.11 s	7.17 s	7.15 s	7.12 bs
H18	7.19 q	7.24 q	7.20 bs	7.22 q	7.24 q
H10	7.12 s	7.19 s	7.38 s	7.25 s	7.36 bs
H19	7.06 d	6.74 bs	7.02 d	6.72 d	6.78 d
H17	6.49 t	6.74 bs	6.50 t	6.57 t	6.58 t
C9-OCH_3	3.82 s	3.81 s	3.96 s	3.82 s	3.91 s
C8-OCH_3	3.79 s	3.77 s	3.89 s	3.78 s	3.86 s
H5	3.42 bs	3.07 t	3.45 bs	3.28 t	3.35 bs
H1’	-	5.01 d	5.48 d	5.11 d	5.38 d
H2’	-	4.86 bs	4.11 t	4.99 d	4.33 t
H3’	-	3.54 bs	3.72 t	3.98 t	3.95 d
H4’	-	3.00 bs	3.77 t	3.24 t	3.61 bs
H5’	-	3.39 bs	4.01 d	3.45 d	3.67 bs

a. See Figures 1 and 4 for numbering scheme.

b. There was a 3:1 doubling of the resonances of JNJ-10148409 suggesting the presence of two rotomers on the NMR timescale.

c. bs denotes a broad singlet, s denotes a sharp singlet, d denotes a doublet, t denotes a triplet, q denotes a quartet, m denotes a multiplet and n.d. denotes not detected.

Table 2: *Carbon (^{13}C) NMR chemical shift Assignment (ppm) of JNJ-10148409 and its glucuronides (temperature 300K)*

Carbon Number[a]	JNJ-10148409 DMSO-d_6 (ppm)	Glu-A CD_3OD (ppm)	Glu-B CD_3OD (ppm)	Glu-C CD_3OD (ppm)
C3	143.5	n.d.	148.9	140.7
C4	110.6	121.0	118.1	115.9
C5	31.2	30.4	32.0	32.3
C6	141.6	140.0	145.3	144.5
C7	110.2	111.7	112.8	112.3
C8	151.1	150.5	151.3	151.9
C9	149.3	150.5	151.0	151.4
C8-O$\underline{C}H_3$	56.6	57.1	58.9	58.6
C9-O$\underline{C}H_3$	56.5	57.1	58.6	58.6
C10	105.0	104.8	107.2	106.4
C11	122.4	128.6	127.3	129.4
C12	154.5	160.0	153.7	163.3
C14[b]	143.6	143.4	148.0	148.6
C15[b]	105.2	106.8	105.5	105.5
C16[b]	163.7	165.3	166.6	166.8
C17[b]	108.8	109.4	108.5	109.4
C18[b]	131.7	131.7	133.1	133.5
C19	114.4	115.5	114.7	114.6
C1’	-	89.7	90.8	88.0
C2’	-	72.6	75.3	74.3
C3’	-	78.2	79.6	80.1
C4’	-	79.7	80.9	80.7
C5’	-	73.7	75.2	75.0
C5’-$\underline{C}O_2H$	-	176.7	178.0	173.0

a. See Figures 1 and 4 for numbering scheme.
b. Since carbons C14, C15, C16, C17 and C18 were doubled due to ^{19}F-^{13}C coupling, the average chemical shifts are reported.

Table 3. *Kinetic constants of Glucuronidation of JNJ-10198409 in HLM*

	$K_{m\ 1}$ (μM)	$V_{max\ 1}$ (nmole min^{-1} mg^{-1})	V_{max}/K_m (nmole min^{-1} mg^{-1}/μM)
Glu-A	1.2	2002	1668
Glu-B	5.0	2403	481

Table 4. *Glucuronide formation rates of individual UGTs*

UGT	Glu-A formation rate (nmole min^{-1} mg^{-1})	Glu-B formation rate (nmole min^{-1} mg^{-1})
1A1	146	155
1A3	41	1003
1A4	576	816
1A6	n.d.	n.d.
1A7	1344	834
1A8	1361	144
1A9	1869	2384
1A10	98	n.d.
2B4	n.d.	n.d.
2B7	n.d.	n.d.
2B15	n.d.	n.d.
2B17	n.d.	n.d.

n.d. denotes insignificant glucuronidation, and rates were not determined.

Table 5. *Kinetic constants of Glucuronidation of JNJ-10198409 by individual UGTs*

UGT	Glu-A formation		Glu-B formation	
	K_m (μM)	V_{max} (nmole min^{-1} mg^{-1})	K_m (μM)	V_{max} (nmole min^{-1} mg^{-1})
1A3	n.d.	n.d.	103.2	2066
1A4	32.7	791	45.9	1204
1A7	2.0	1508	3.1	852
1A8	8.6	1704	16.2	171
1A9	2.0	1772	3.4	2456

n.d. denotes insignificant glucuronidation, and rates were not determined.

Table 6. *Propofol(100 μM) inhibition of Glucuronidation of JNJ-10198409 in HLM*

Drug concentartion (μM)	Glu-A formation* (%)	Glu-B formation* (%)
0	100	100
1	11	13
5	87	93
25	104	107

- Glucuronide formation was expressed relative to the control group (no inhibitor).

DMD Fast Forward. Published on February 2, 2006 as DOI: 10.1124/dmd.106.009274
This article has not been copyedited and formatted. The final version may differ from this version.

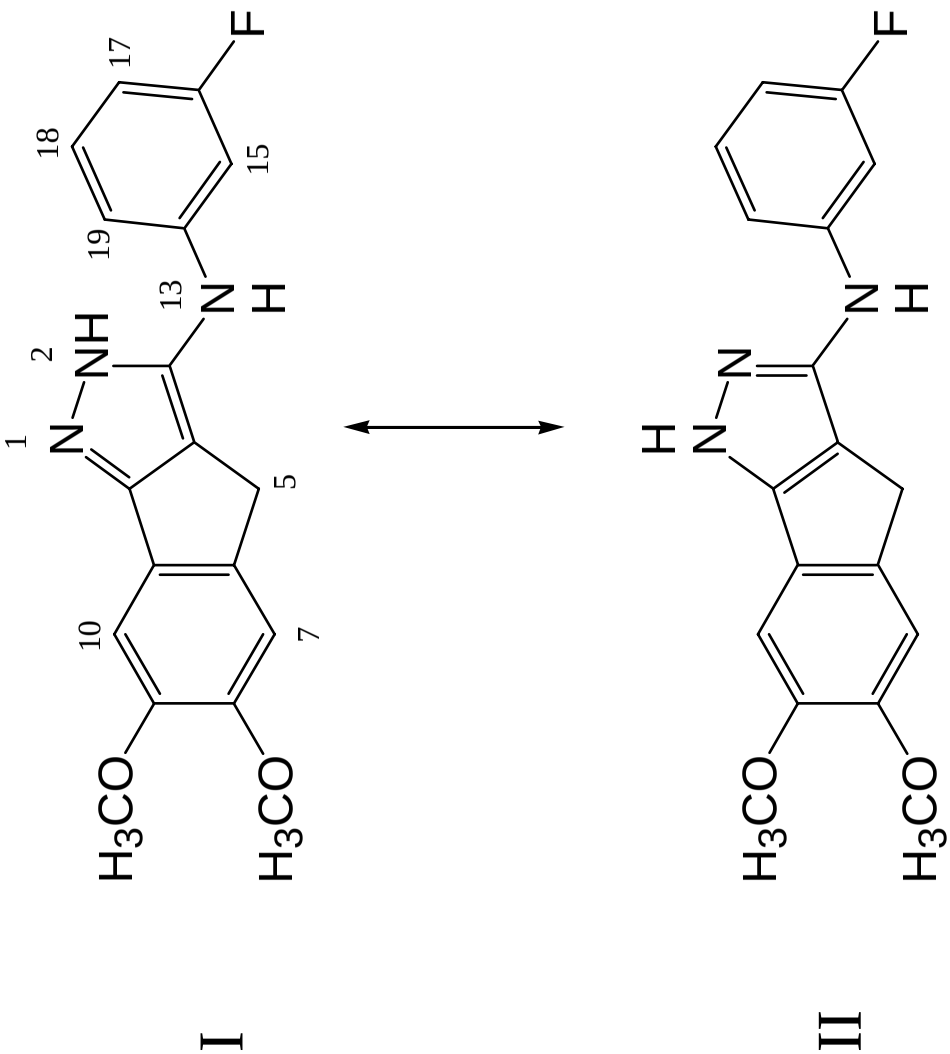

Figure 1

Figure 2A, B

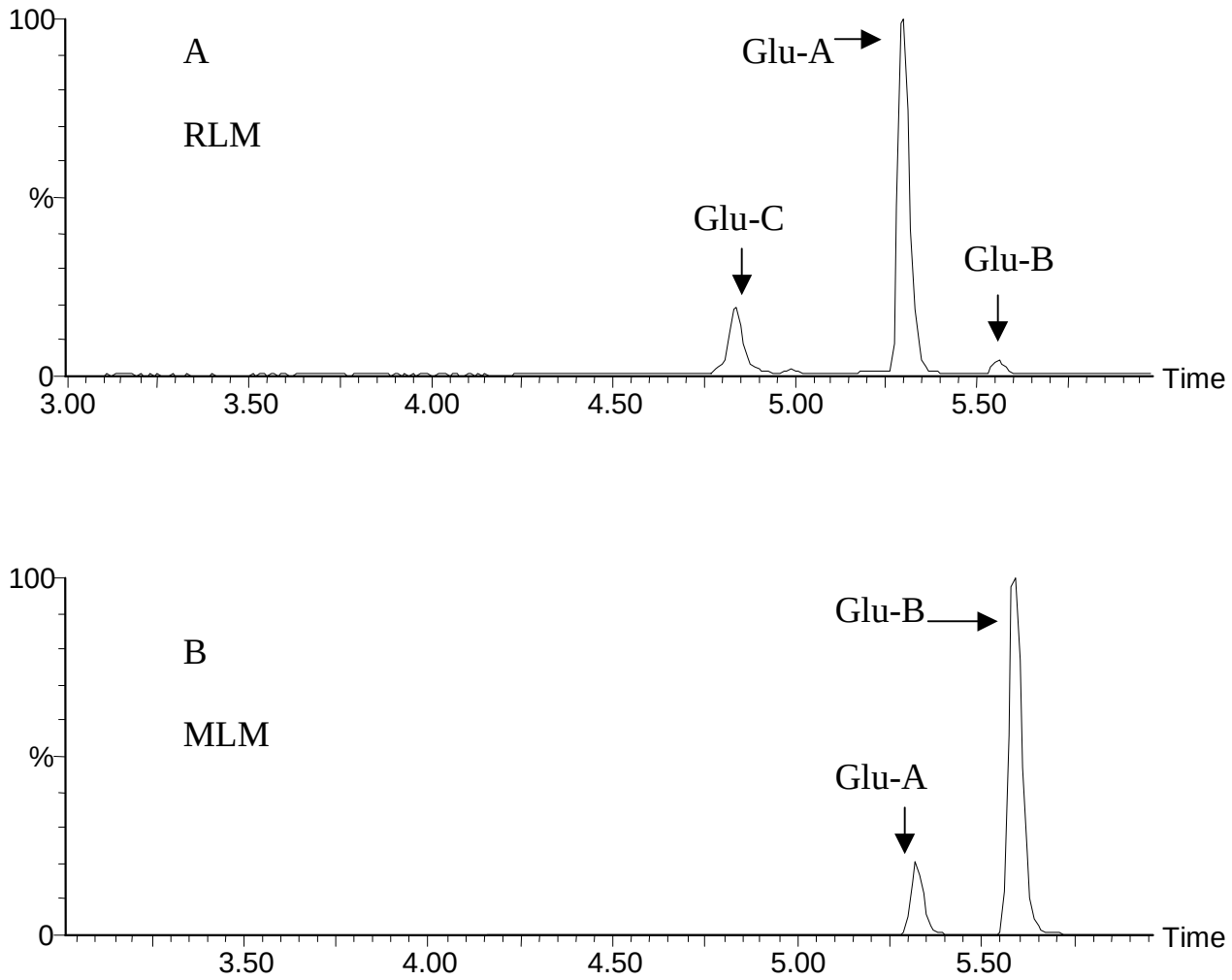

Figure 2C

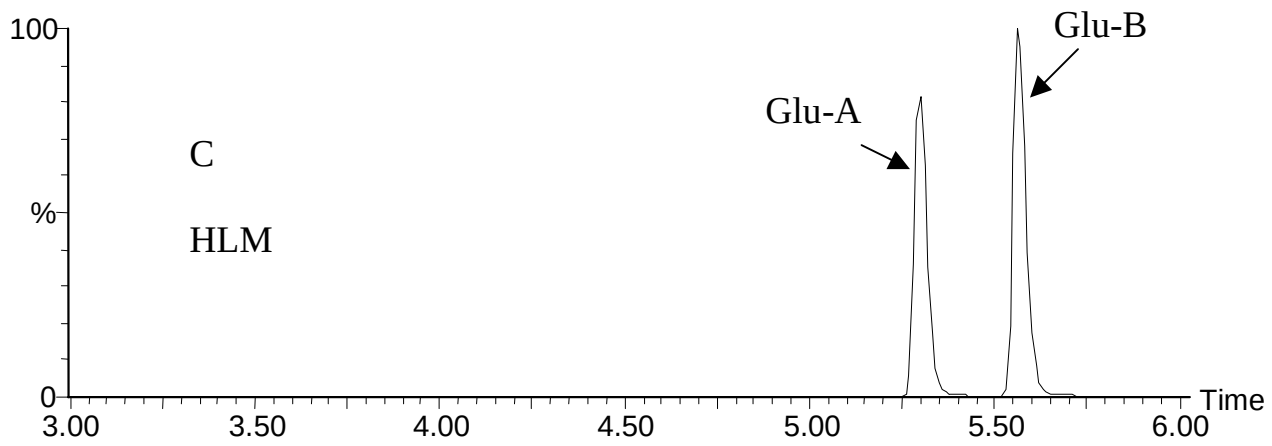

Figure 3A,B

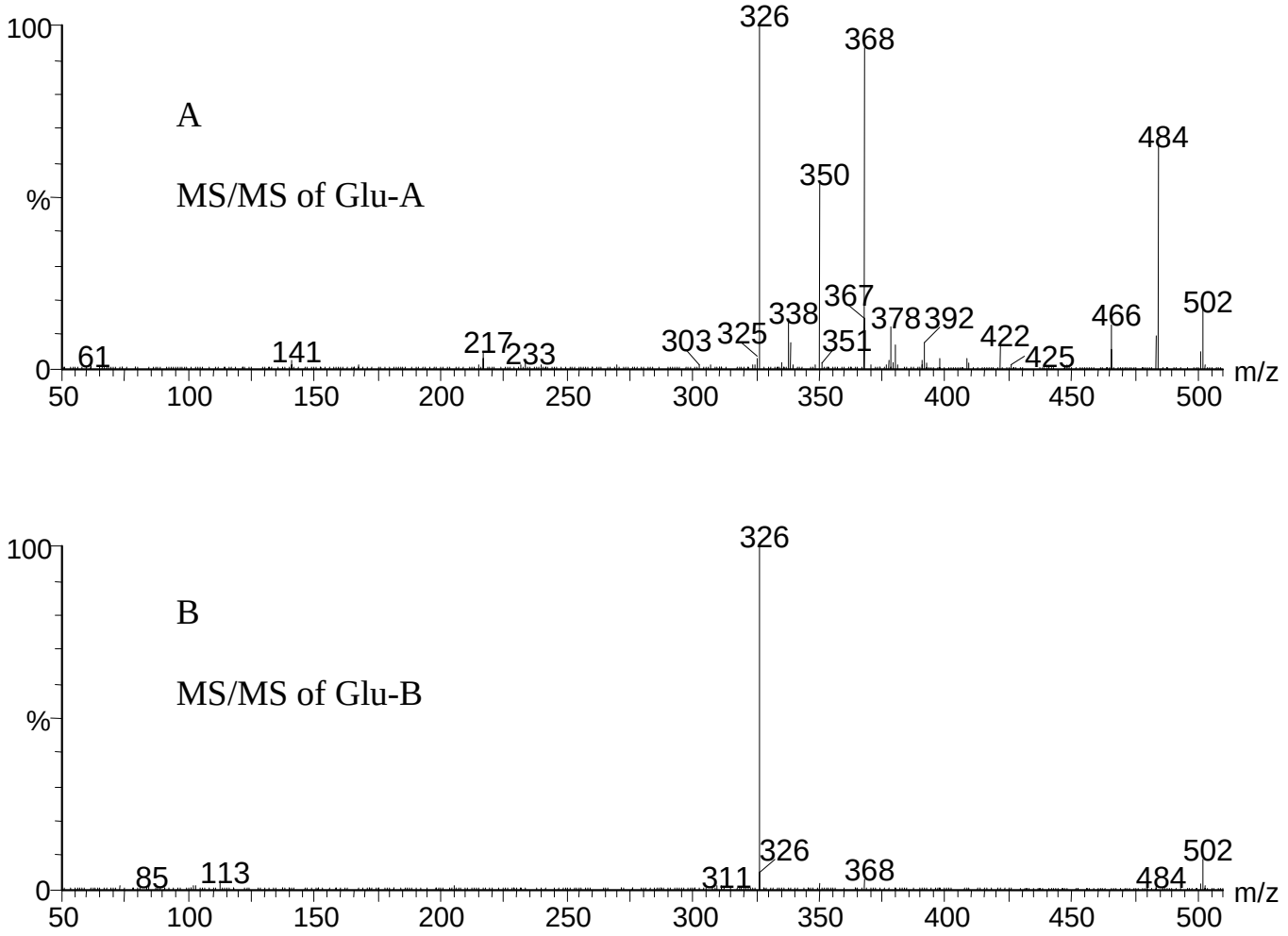

Figure 3C

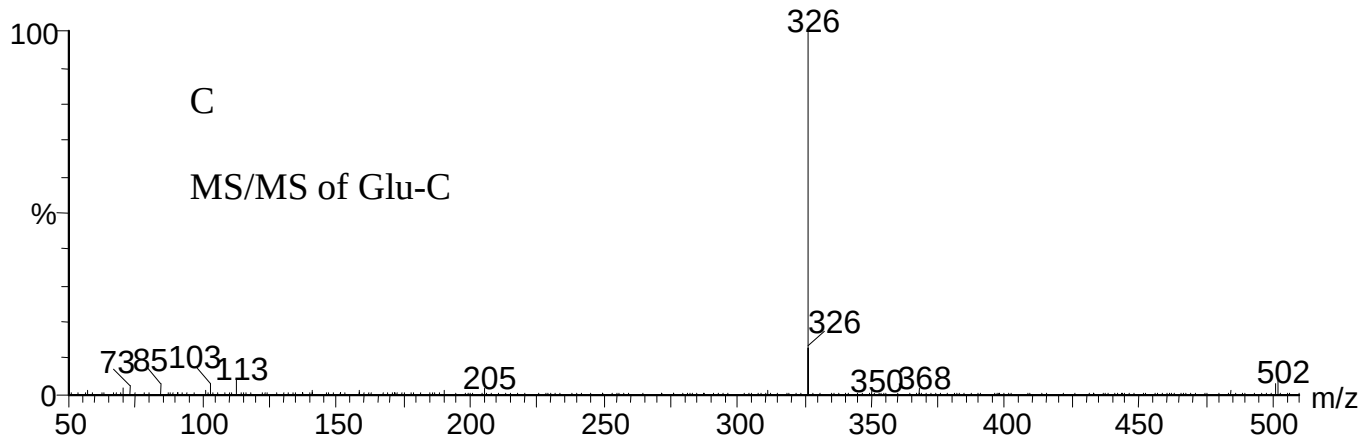

Figure 4

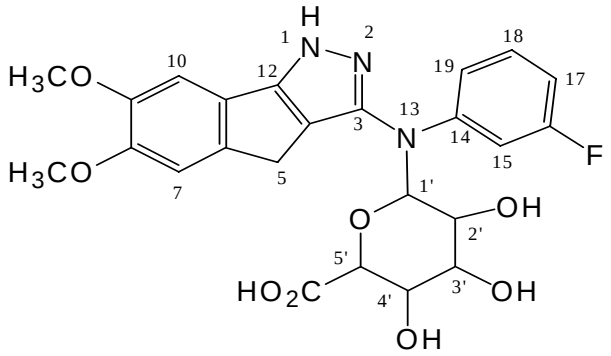

(Glu-A)

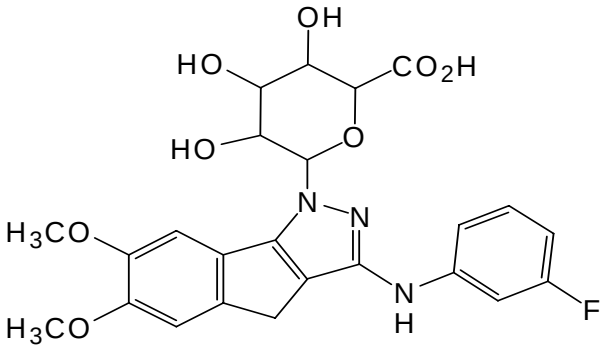

(Glu-B)

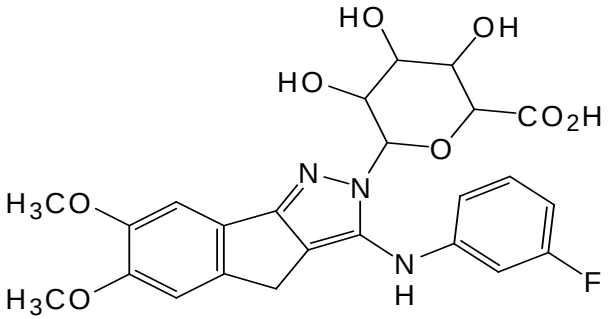

(Glu-C)

Figure 5

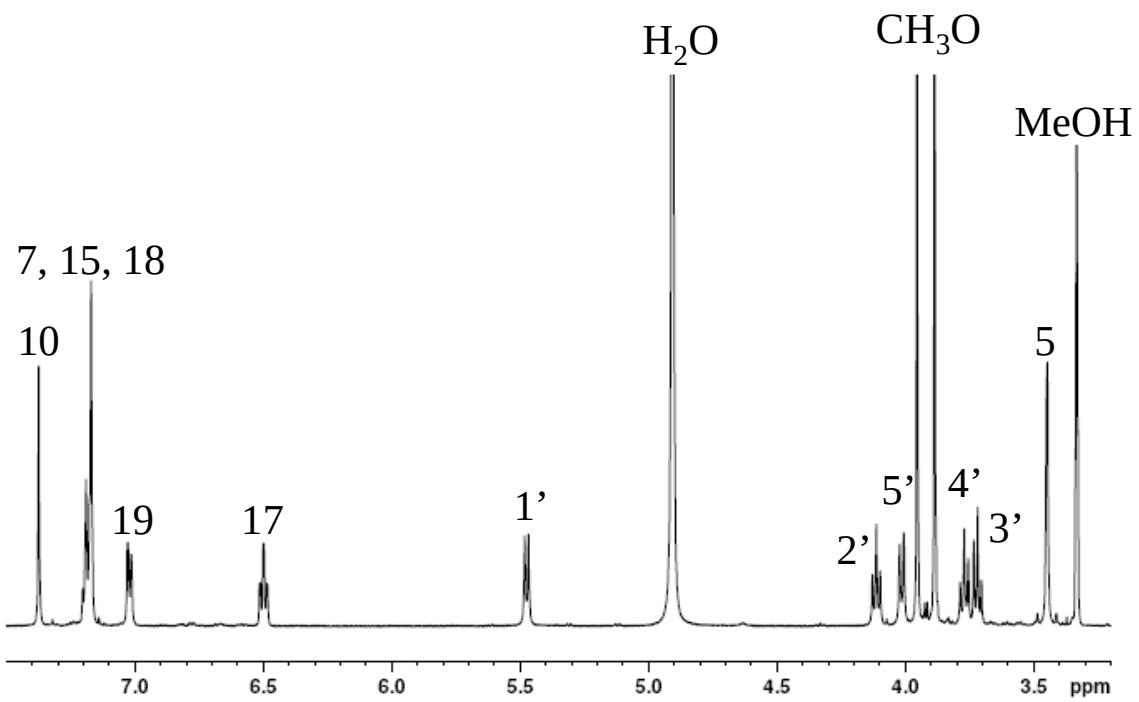

Figure 6A

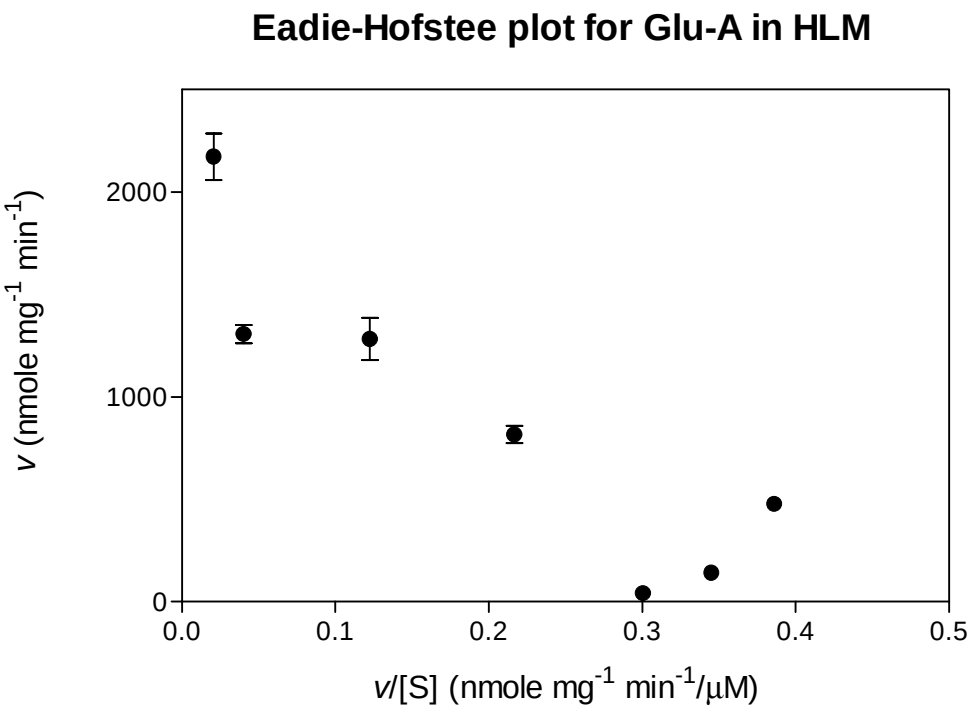

Figure 6B